Journal of Power Sources 206 (2012) 409–413

Contents lists available at SciVerse ScienceDirect

Journal of Power Sources

journal homepage: www.elsevier.com/locate/jpowsour

Short communication

A composite of sulfur and polypyrrole–multi walled carbon combinatorial nanotube as cathode for Li/S battery

Xiao Liang, Zhaoyin Wen*, Yu Liu, Hao Zhang, Jun Jin, Meifen Wu, Xiangwei Wu

CAS Key Laboratory of Energy Transforming Materials, Shanghai Institute of Ceramics, Chinese Academy of Sciences, Shanghai 200050, PR China

ARTICLE INFO

Article history:
Received 24 September 2011
Received in revised form 20 January 2012
Accepted 21 January 2012
Available online 28 January 2012

Keywords:
Polypyrrole–multi walled carbon tube composites
Chemical oxidation
Sulfur cathode
Lithium battery

ABSTRACT

A core/shell structure of polypyrrole (PPy) and multi walled carbon tube (MWCNT) composite is proposed. The PPy is introduced to the surface of MWCNT by an in situ polymerization of pyrrole with $FeCl_3$ as the oxidizing agent. The structures of the PPy–MWCNT composites are analyzed by Raman spectra. The surface area of the PPy–MWCNT composite increases with the increase of the PPy content in the composite. Adversely, the conductivity of the S/PPy–MWCNT decreases. The MWCNT provides the high electronic conductive network. Meanwhile, the PPy with high surface area ensures an uniform dispersion of the sulfur. As a result, S/PPy–MWCNT with 25 wt.% PPy shows the discharge capacity of 725.8 mA h g^{-1} after 100 cycles.

1. Introduction

Lithium/sulfur battery is attractive for its highest theoretical specific capacity of 1675 mA h g^{-1} and high theoretical specific energy of 2600 W h kg^{-1} among all the solid cathode lithium battery system [1]. In a typical Li/S system, elemental sulfur serves as the active cathode material and lithium metal as the anode. Sulfur undergoes reduction by lithium to form a series of polysulfides (Li_2S_8–Li_2S_2) and then Li_2S, which corresponds to 100% depth of discharge [2,3]. The reaction is highly reversible. In addition, sulfur has the advantages of low cost, low toxicity and abundance [4]. So, lithium sulfur is the most promising system for the next generation of high energy rechargeable lithium battery. However, elemental sulfur is electrically and ionically insulating, leading to a poor electrochemical activity of the sulfur cathode [5]. Moreover, numerous attentions have been paid to low utilization of active material, poor recharge ability and dissolution of polysulfides into the electrolyte [6,7]. The dissolved polysulfides diffuse through the electrolyte to the lithium anode where they are reduced to form solid precipitates such as Li_2S_2 or Li_2S. These reduced products can also diffuse back to the cathode by charging. This shuttle phenomenon could lead to the lithium corrosion and finally the capacity fading [8].

To avoid these disadvantages, conductive agents with special structures were added to the sulfur cathode to alleviate the dissolution of polysulfides. Porous carbon with bimodal pore structure was proposed as the conducting agent in the sulfur cathode, and the small mesopores contain the majority of the sulfur and polysulfide while the large interconnected pores favor the rapid transport of solvated Li^+ on charge/discharge [9,10]. Ordered mesoporous carbon CMK-3 was reported to act both as the conducting agent and the host to contain active sulfur [11,12]. Graphene is favorable for its high surface area and conductivity, but the preparation is complicated and expensive [13–16]. Conductive polymer is profitable for its compatibility with the sulfur and organic electrolyte. Polythiophene was coated on the sulfur particle and effectively enhanced the performance of the lithium sulfur battery [17]. Multi-walled carbon tube (MWCNT) is attractive for its high conductivity and unique structure. It is reported that MWCNT could improve the long time cycling performance of the lithium sulfur battery [18]. However, it is difficult to obtain uniformly dispersed sulfur in the MWCNT [19]. In our previous studies, we found that polypyrrole (PPy) has great absorbing ability to the sulfur and polysulfides, which can help to hold back the solubility of polysulfides [20,21].

In this study, a core/shell structure of PPy and MWCNT was proposed. The PPy was introduced to the surface of MWCNT by an in situ polymerization of pyrrole with $FeCl_3$ as the oxidizing agent. The unique core/shell structure with effective conductive network provided by the MWCNT as well as the strong absorbility to sulfur and polysulfides provided by PPy enables the homogenous dispersion of the sulfur, facilitates the transportation of ions and improves the cycling performance of the lithium sulfur battery.

* Corresponding author. Tel.: +86 21 5241 1704; fax: +86 21 5241 3903.
E-mail address: zywen@mail.sic.ac.cn (Z. Wen).

0378-7753/$ – see front matter © 2012 Elsevier B.V. All rights reserved.
doi:10.1016/j.jpowsour.2012.01.123

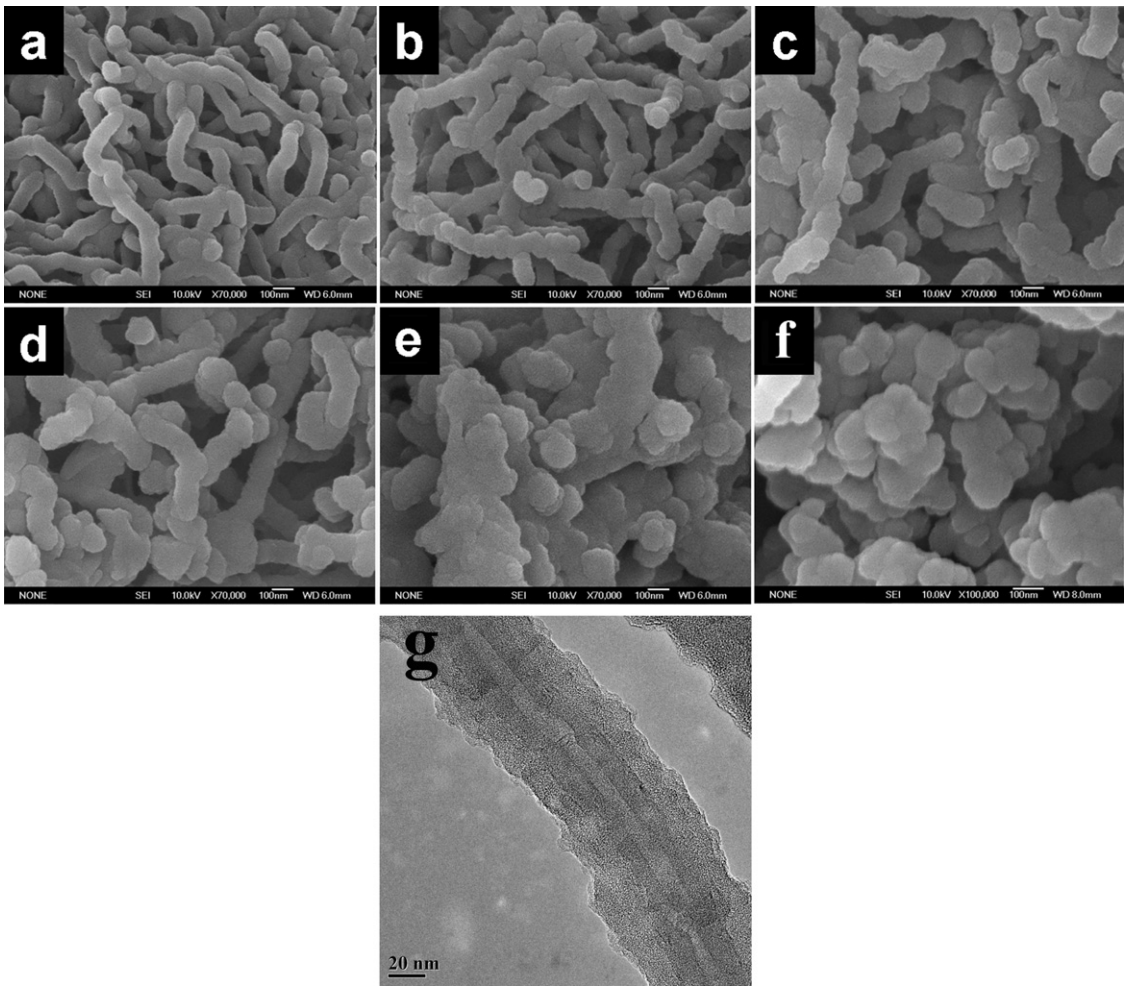

Fig. 1. SEM micrographs of: (a) Pure MWCNT, (b) PPy–MWCNT with 10 wt. PPy, (c) PPy–MWCNT with 25 wt.% PPy, (d) PPy–MWCNT with 40 wt.% PPy, (e) PPy–MWCNT with 60 wt.% PPy, (f) pure PPy. The scale bar is 100 nm, and (g) TEM graph of PPy–MWCNT composite with 25 wt.% PPy.

2. Experimental

PPy–MWCNT with different PPy contents was synthesized by an in situ chemical oxidative polymerization of pyrrole on MWCNT. Firstly, MWCNT was dispersed in 100 ml water with 0.1 M cetyltrimethylammonium bromide (CTAB) by sonication for 2 h. Then, pyrrole was dropped into the solution and stirred for 30 min by magnetic stirring. After that, proper amount of $FeCl_3$ (three times as much as the mole of the pyrrole) was added by dropping and stirred for 4 h. The product was washed and filtered until the filtrate was colorless. The PPy–MWCNT composites were dried under vacuum at 80 °C for 12 h. S/PPy–MWCNT composites prepared as the follows: the mixture of sulfur and PPy–MWCNT was mixed with weight ratio of 7:3 before sealed in a glass tube under Ar protection. Then the glass tube was heated at 155 °C for 4 h. After it cooled to room temperature, the glass tube was opened carefully.

The S/PPy–MWCNT composites with 70 wt.% S was mixed with acetylene black and PVDF (polyvinylidenefluoride), using NMP (N-methyl-2-pyrrolidone) as the dispersant. The weight ratio of sulfur composite, acetylene and PVDF in the mixture is 70:10:20. The slurries were cast onto aluminum foil substrates. After the organic solvent was evaporated, the electrode film was cut to sheets of 14 mm in diameter and then dried at 50 °C under vacuum for 12 h.

Field emission scanning electron microscope (FESEM JSM-6700) and transmission electron microscope (TEM JEM-2010) were applied to observe the morphology of the synthesized composite material. Raman spectroscopy was recorded on a DXR Raman Microscope with 532 nm excitation length (Thermal Scientific Co., USA). Specific surface area was tested using the Brunauer–Emmett–Telley (BET) method on the Micromeritics Tristar 3000. Thermogravimetry (TG) (NETZSCH 409 PC) was applied to determine the components of the composite. Phase analyses were

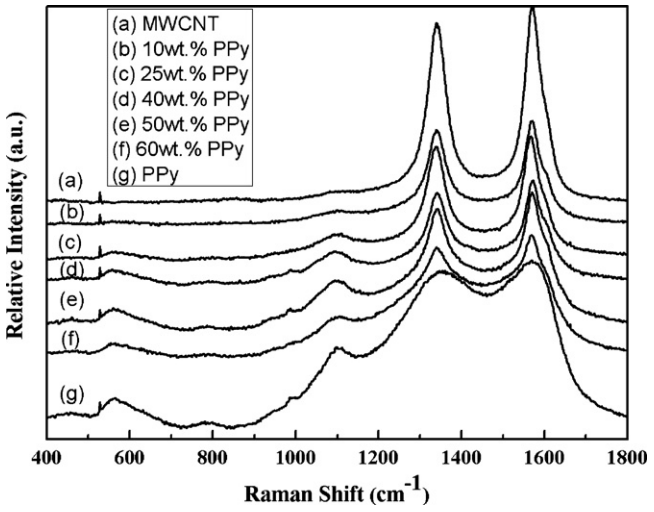

Fig. 2. Raman spectra of the Pure PPy, MWCNT and the as prepared PPy–MWCNT composites.

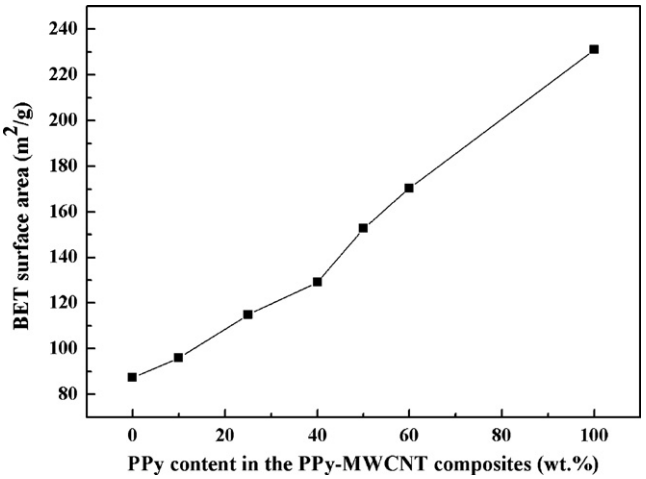

Fig. 3. BET surface area of the Pure PPy, MWCNT and the as prepared PPy–MWCNT composites with different PPy content.

conducted by X-ray diffraction (XRD, Rigaku RINT-2000) with Cu Kα radiation.

CR2025 type coin cells were assembled in a glove box with oxygen and water contents less than 1 ppm. A solution of 1 M $LiCF_3SO_3$ dissolved in tetra(ethylene glycol) dimethyl ether (TEGDME) was employed as the electrolyte. The cells contained Celgard 2400 as the separator and lithium foils as the counter and reference electrodes. AC impedance was measured by a Frequency Response Analyzer (FRA) technique on an Autolab Electrochemical Workstation over the frequency range from 1 MHz to 10 mHz with the amplitude of 10 mV. The galvanostatic charge and discharge tests were conducted on a LAND CT2001A battery test system in the voltage range of 1.0–3.0 V (vs. Li/Li^+) at a current density of 0.1 mA cm^{-2}.

3. Results and discussion

Fig. 1 shows the micrographs of the as prepared PPy–MWCNT composites with different PPy contents. As shown in Fig. 1a, the commercial MWCNT is about 40 nm in diameter, and a couple of micrometers in length. The surface of the MWCNT is relatively smooth. The agglomerated granular pure PPy possesses the primary particles with a diameter of 100 nm, shown in Fig. 1e. After the incorporation of PPy onto the MWCNT, a core–shell structure was obtained. The PPy with high absorbability was coated on the MWCNT. As a result, the diameter of the PPy–coated MWCNT increased with the increasing content of PPy composite, shown in Fig. 1b–d, reaching to about 80 nm in diameter for the PPy–MWCNT with 40 wt.% PPy. Actually, there are some free PPy particles in the PPy–MWCNT with 60 wt.% PPy. It means that when the PPy content in the PPy–MWCNT composites is too large, only part of the PPy was coated on the MWCNT surface. The core–shell structure can be demonstrated clearly by the TEM graph of the PPy–MWCNT with 25 wt.% PPy in Fig. 1g. The well-defined lattice fringes of the MWCNT walls reserve as a core and amorphous PPy is coated on the surface of the MWCNT to serve as the shell.

Fig. 2 shows the Raman spectra of pure PPy and the PPy–MWCNT composites. For comparison, the figure also includes the MWCNT spectrum, which contains two strong peaks at 1580 and 1355 cm^{-1} assigning to tangential mode (G-band) and disorder mode (D-band), respectively [22]. The intensity of these two peaks gradually increases for the PPy–MWCNT composites as the MWCNT content increases. Meanwhile, the characteristic peak for PPy of quinonoid polaronic structure at 1086 cm^{-1} decreases. Also, the decreasing peak at 1086 cm^{-1} reveals that parts of PPy have not fully reacted with MWCNT [23].

The specific areas of the composites were tested by BET method, as shown in Fig. 3. The specific area of the composite increases with the increases of PPy content, implying that the PPy coated on the MWCNT exhibits a porous structure. The specific area increased rapidly when the PPy content is larger than 40 wt.%. Compared with

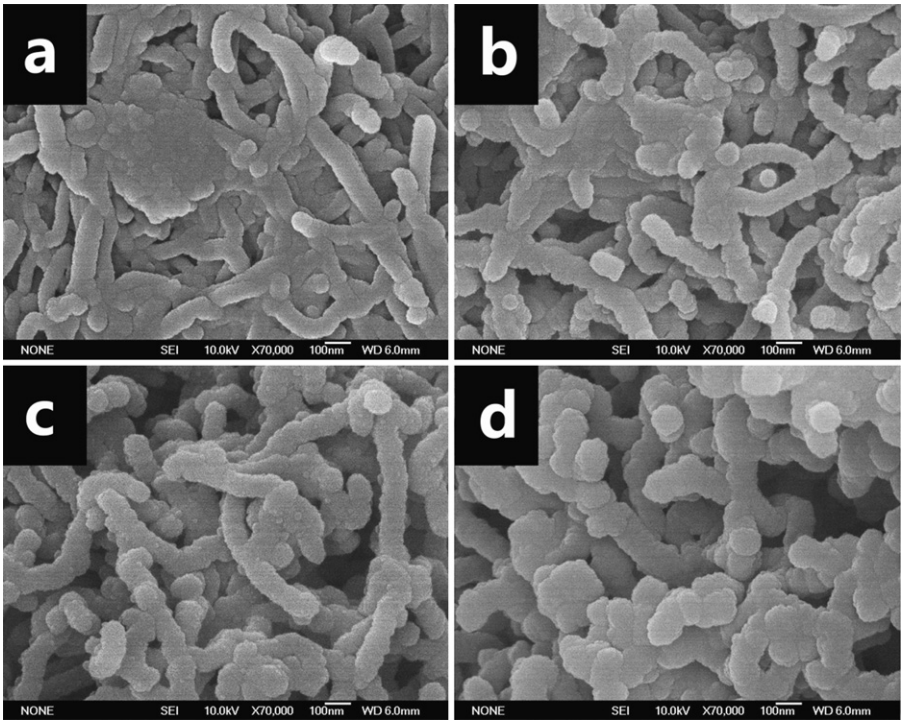

Fig. 4. Morphology of: (a) S/MWCNT, (b) S/PPy–MWCNT with 10 wt.% PPy, (c) S/PPy–MWCNT with 25 wt.% PPy and (d) S/PPy–MWCNT with 40 wt.% PPy. The scale bar is 100 nm.

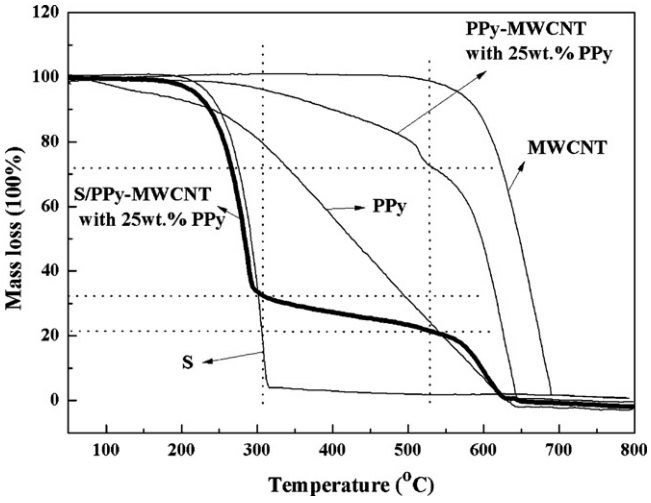

Fig. 5. TG curves of the MWCNT, PPy, S, PPy–MWCNT with 25 wt.% PPy and S/PPy–MWCNT with 25 wt.% PPy.

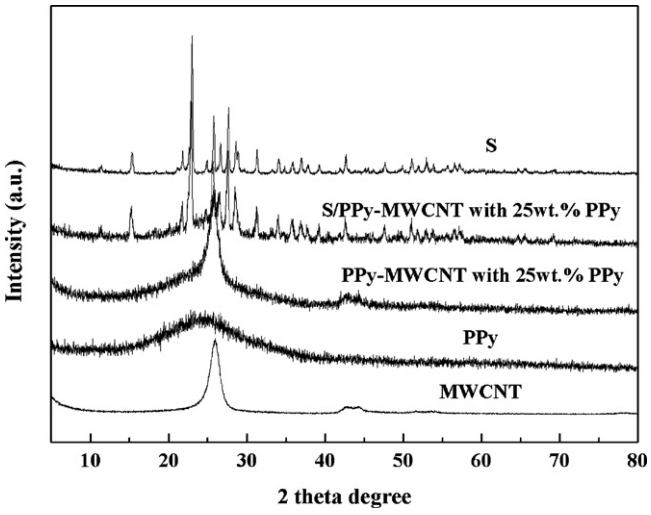

Fig. 6. XRD patterns of MWCNT, PPy, PPy–MWCNT, S/PPy–MWCNT and sulfur.

the SEM morphologies in Fig. 1, the free PPy particles out of the core–shell structure are supposed to lead to the fast increase of the specific area.

Fig. 4 shows the SEM micrographs of the S/PPy–MWCNT composites. The greatest difference between the S/MWCNT and S/PPy–MWCNT is the significant sulfur aggregation in the S/MWCNT composite. However, no sulfur aggregation is observed in the S/PPy–MWCNT composites. It means that the structure of PPy–coated MWCNT is favorable for the dispersion of sulfur. The TG curves of the PPy, MWCNT, PPy–MWCNT with 25 wt.% PPy as well as S/PPy–MWCNT with 25 wt.% PPy are shown in Fig. 5. PPy content in the PPy–MWCNT is about 25 wt.%, and the sulfur content in the S/PPy–MWCNT composite is about 70 wt.%, which are consistent with its original ratio of components. Fig. 6 shows the XRD patterns of the composite. The sulfur in the S/PPy–MWCNT composite belongs to the Fddd orthorhombic crystal system, indicating that the sulfur loading process on the PPy–MWCNT composite dose not bring any structure change.

As shown in Fig. 7a, there are two main peaks near 2.3 V and 1.9 V in the cathodic process corresponding to the change from element sulfur to the higher-order lithium polysulfides (Li_2S_n, $n \geq 4$) and then to lower-order polysulfides ($n < 4$) until Li_2S, respectively [24]. At the following cycles, the cathodic peaks are shifted to higher

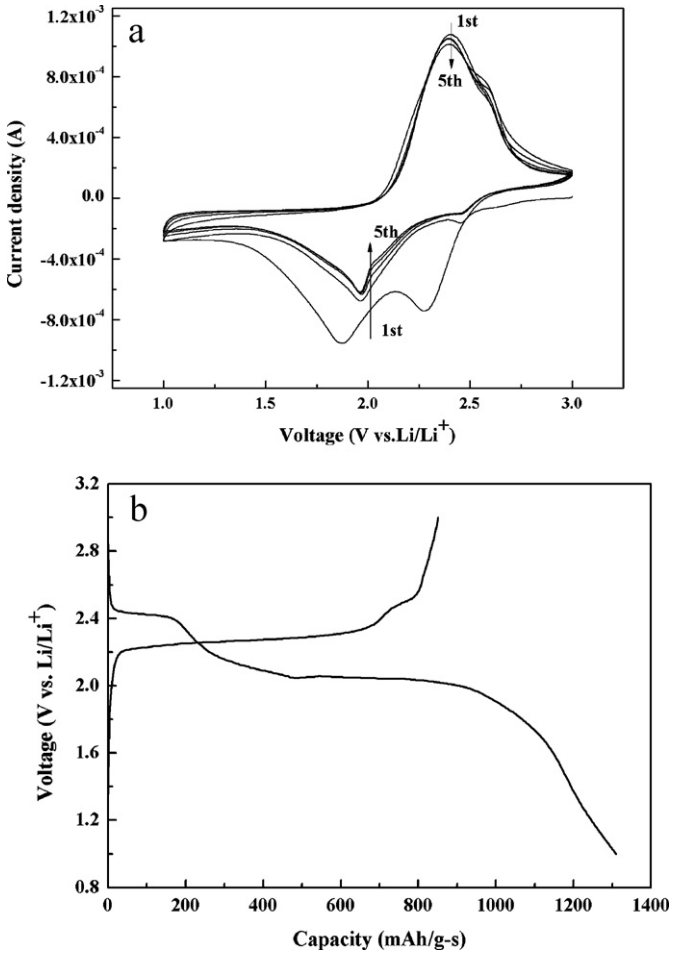

Fig. 7. CV curve (a) and the initial discharge/charge curve (b) of the S/PPy–MWCNT.

voltage. It is owing to the electrochemical reactions during the first discharge process needing overcome the strong absorbing energy between the sulfur and the conductive matrix [26]. The voltage and peak current density of the cathodic and anodic peaks for the composite keeps constant after 2nd cycles, showing the stable performance of the composite. The discharge curves of the composites shown in Fig. 7b present two voltage plateaus, which matches with the CV curves. The S/PPy–MWCNT shows an initial discharge capacity of ca. 1309 mA h g^{-1}, but the charge capacity is only ca. 852 mA h g^{-1}. The intrinsic low initial discharge–charge efficiency may originate from the solid electrolyte interface (SEI) on the lithium anode which is built at the first few charge processes. Additionally, the volume change of the sulfur cathode during cycling may lead to the poor contact of the cathode with the current collector and thus the low charge capacity [25].

The AC impedances of the S/PPy–MWCNT composites with different PPy contents are shown in Fig. 8. The impedance spectra are composed of a semi-circle in the high frequency region corresponding to the contact resistance and charge transfer resistance, as well as a short inclined line in the low frequency region due to the ion diffusion within the electrode. The S-MWCNT shows the lowest charge transfer resistance. The resistance of the composite increased gradually with the increase of PPy content in the composite. Since the carbon tube provides a higher electronic conductivity than PPy and forms conductive networks. As a result, higher the MWCNT content in the PPy–MWCNT, higher the conductivity of the S/PPy–MWCNT cathode.

Fig. 9 shows the cycling performance of the S/PPy–MWCNT composites. As seen, the composite with 10 wt.% PPy presents the

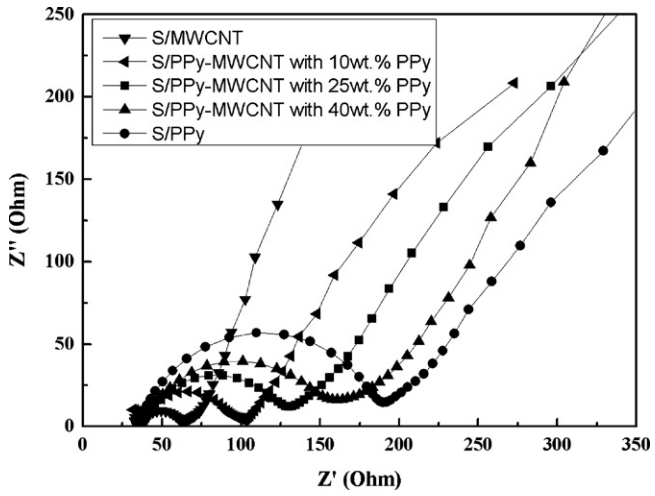

Fig. 8. AC impedance spectra of the S/PPy electrode, S/MWCNT electrode and S/PPy–MWCNT composite with different PPy contents. The frequency is 0.01–10^6 Hz.

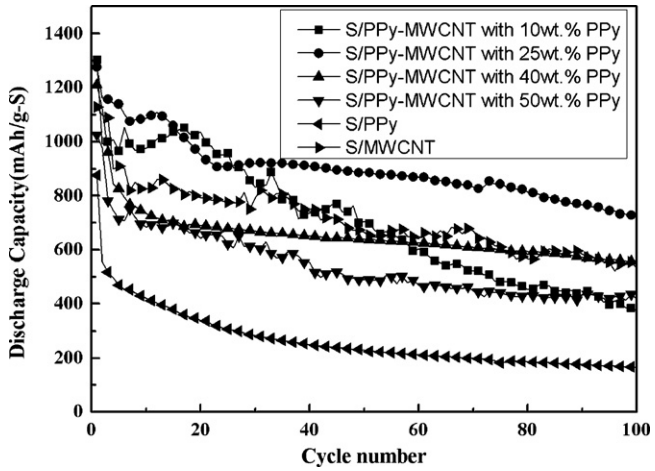

Fig. 9. Cycling performance of the S/PPy–MWCNT with different PPy contents in 1 M $LiCF_3SO_3$ – TEGDME electrolyte.

highest initial discharge capacity of 1303 mA h g^{-1}, corresponding to 77.8% sulfur utilization. The initial discharge capacity of the S/PPy–MWCNT composite decreased with the increase of the PPy content in the composite, meaning that the initial discharge capacity is significantly influenced by the conductivity of the cathode. The S/PPy–MWCNT with 25 wt.% PPy shows the best cycling performance with the discharge capacity of 725.8 mA h g^{-1} after 100 cycles, about 56% retention of the initial discharge capacity of about 1275 mA h g^{-1}. Taking account of the results in Figs. 3 and 8, good performance of the composite can be ascribed to the combination of the surface area and impedance of the PPy–MWCNT. The MWCNT provides the high conductivity network. Meanwhile, the PPy with high surface area ensures uniform dispersion of the sulfur as well as strong adsorption to the polysulfides. Though pure PPy has the highest surface area, the high resistance of the S/PPy leads to the low initial discharge capacity and the fast capacity fading.

4. Conclusion

A core/shell structure of PPy–MWCNT composites with different PPy contents was synthesized by the in situ chemical oxidation of PPy on the surface of MWCNT. With the increase of PPy content, the surface area of the PPy–MWCNT composite increases, but the conductivity decreases. The S/PPy–MWCNT composite with 25 wt.% PPy shows the highest discharge capacity of 725.8 mA h g^{-1} after 100 cycles, about 57% of the initial discharge capacity.

Acknowledgments

This work was financially supported by NSFC Project Nos. 50730001 and 50973127, research projects of Chinese Science and Technology Ministry No. 2007CB209700, and research projects from the Science and Technology Commission of Shanghai Municipality Nos. 08DZ2210900 and 09PJ1410800.

References

[1] X. Ji, L.F. Nazar, Mater. Chem. J. 20 (2010) 9821–9826.
[2] N. Jayaprakash, J. Shen, S.S. Moganty, A. Corona, L.A. Archer, Angew. Chem. 123 (2011) 1–6.
[3] P.G. Bruce, L.J. Hardwick, K.M. Abraham, MRS Bull. 36 (2011) 506–512.
[4] B. Zhang, X. Qin, G.R. Li, X.P. Gao, Energy Environ. Sci. 3 (2010) 1531–1537.
[5] K. Kumaresan, Y. Mikhaylik, R. White, J. Electrochem. Soc. 155 (2008) A576.
[6] J. Wang, S.Y. Chew, Z.W. Zhao, S. Ashraf, D. Wexler, J. Chen, S.H. Ng, S.L. Chou, H.K. Liu, Carbon 46 (2008) 229–235.
[7] L.X. Yuan, J.K. Feng, X.P. Ai, Y.L. Cao, S.L. Chen, H.X. Yang, Electrochem. Commun. 8 (2006) 610–614.
[8] Y.V. Mikhaylik, J.R. Akridge, J. Electrochem. Soc. 151 (2004) A1969–A1976.
[9] G. He, X.L. Ji, Nazar Linda, Energy Environ. Sci. 4 (2011) 2878–2883.
[10] C.D. Liang, N.J. Dudeny, J.Y. Howe, Chem. Mater. 21 (2009) 4724–4730.
[11] X.L. Ji, K.T. Lee, L.F. Nazar, Nat. Mater. 8 (2009) 500.
[12] S.R. Chen, et al., Electrochim. Acta (2011), doi:10.1016/j.electacta.2011.03.005.
[13] H.L. Wang, Y. Yang, Y.Y. Liang, J.T. Robinson, Y.G. Li, A. Jackson, Y. Cui, H.J. Dai, Nano Lett. 11 (2011) 2644–2647.
[14] J.Z. Wang, et al., J. Power Sources (2010), doi:10.1016/j.jpowsour.2010.09.106.
[15] Y.L. Cao, X.L. Li, I.A. Aksay, J. Lemmon, Z.M. Nie, Z.G. Yang, J. Liu, Phys. Chem. Chem. Phys. 13 (2011) 7660–7665.
[16] J.Z. Wang, L. Lu, M. Choucair, John A. Stride, X. Xu, H.K. Liu, J. Power Sources 196 (2011) 7030–7034.
[17] F. Wu, J.Z. Chen, R.J. Chen, S.X. Wu, L. Li, S. Chen, T. Zhao, J. Phys. Chem. C 115 (2011) 6057–6063.
[18] L.C. Yin, J.L. Wang, J. Yang, Y.N. Nuli, J. Mater. Chem. 21 (2011) 6807–6810.
[19] Y. Choi, K. Kim, H. Ahn, J. Ahn, J. Alloys Compd. 449 (2008) 313–316.
[20] X. Liang, Y. Liu, Z.Y. Wen, X.Y. Wang, H. Zhang, M.F. Wu, L.Z. Huang, Solid State Ionics 192 (2011) 347–350.
[21] X. Liang, Y. Liu, Z.Y. Wen, L.Z. Huang, X.Y. Wang, H. Zhang, J. Power Sources 196 (2011) 6951–6955.
[22] N.G. Sahoo, Y.C. Jung, H.H. So, J.W. Cho, Synth. Met. 157 (2007) 374–379.
[23] T.M. Wu, S.H. Lin, J. Polym. Sci. Part B: Polym. Phys. 44 (2006) 1413–1418.
[24] D. Marmorstein, T.H. Yu, K.A. Striebel, E.J. Cairns, J. Power Sources 89 (2000) 219–226.
[25] X.M. He, J.G. Ren, L. Wang, W.H. Pu, C.Y. Jiang, C.R. Wan, J. Power Sources 190 (2009) 154–156.
[26] B. Zhang, C. Lai, Z. Zhou, X.P. Gao, Electrochim. Acta 54 (2009) 3708.